

# A Measured Look at Neuronal Oxygen Consumption

John E. W. Mayhew

Neuroscientists have long disputed whether activated neurons in the brain significantly increase their consumption of oxygen, or whether they exploit anaerobic metabolism for energy production. An elegant contribution from Thompson *et al.* on page 1070 of this issue (1) answers this question directly. In doing so, these authors make an important contribution to our understanding of a sophisticated brain imaging technique that pinpoints regions of neural activity by detecting changes in tissue oxygenation and blood volume.

After neural activation (particularly in the cerebral cortex), an increase in blood flow produces an influx of oxygenated hemoglobin. This influx reduces the local concentration of deoxygenated hemoglobin (deoxyhemoglobin). This reduction can be measured by a sophisticated imaging technique called BOLD fMRI (blood oxygen level-dependent functional magnetic resonance imaging). BOLD fMRI is used to pinpoint specific brain areas that are activated when certain tasks are performed (2). However, a paradox of the BOLD response is that the amount of oxygen supplied to activated neural tissue by the increase in blood flow seems far greater than would be required simply to meet the metabolic needs of the tissue.

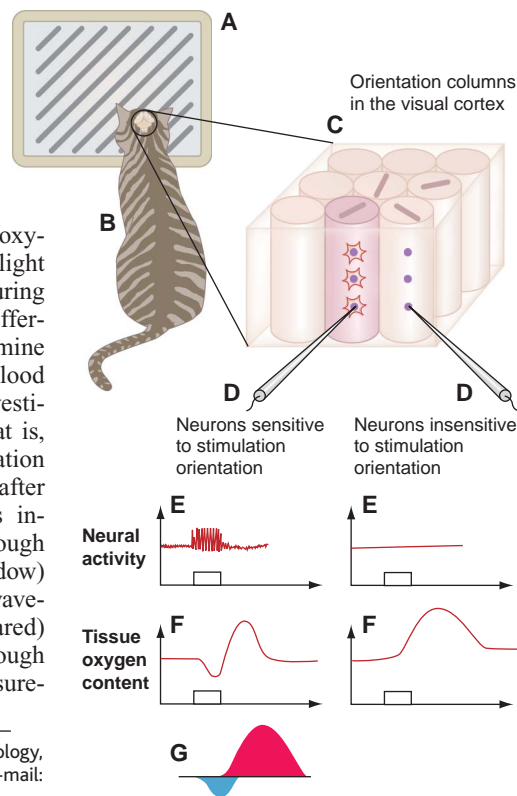
Optical imaging spectroscopy exploits the fact that oxygenated and deoxygenated hemoglobin have different light absorption spectra (3–5). By measuring changes in remitted illumination at different wavelengths, it is possible to determine changes in tissue oxygenation and blood volume. Many experiments have investigated the hemodynamic response (that is, changes in blood volume and oxygenation resulting from increased blood flow) after neural activation. These experiments involved viewing the exposed brain through a small hole in the skull (cranial window) illuminated with light at visible wavelengths. Light of longer (near infrared) wavelengths can be used to “see” through the skull enabling noninvasive measure-

ments to be made. Optical imaging spectroscopy has revealed an early rise in the deoxyhemoglobin concentration of the rat and cat cortex after exposure to various stimuli (3–5). This finding suggested that the metabolic demands of activated neurons were being met by an increase in aerobic metabolism. Similarly, subsequent BOLD fMRI studies showed a transient increase in the concentration of deoxyhemoglobin (often referred to as the “initial dip” in the BOLD signal) after stimulation of the visual cortex in humans (6, 7).

The “initial dip” component of the BOLD response has been exploited to delineate areas of the cat visual cortex called ocular dominance columns. (Ocular dominance columns are regions of the visual cortex where neurons show preferential sensitivity to inputs from one eye over the other. Within ocular dominance columns there are orientation columns where neurons at different depths show the same preferential sensitivity to a stimulus at a partic-

ular orientation.) Earlier optical imaging studies using a single wavelength of illumination revealed that wavelengths more sensitive to changes in deoxyhemoglobin concentration produced higher resolution spatial maps of cortical architecture (8).

Recent work (9, 10) provides more evidence for local changes in the oxygen concentration of brain tissue after neural activation. However, no study has related neural activity to changes in tissue oxygenation with the fine spatial resolution that Thompson *et al.* now report (1). These authors exploit the columnar organization of neurons with similar orientation sensitivities to a narrow range of stimuli in the cat visual cortex. They demonstrate that local tissue oxygenation is reduced following neural activity, and that neurons do in fact increase their oxygen consumption following activation. First, they implanted combined electrodes measuring oxygen concentration and single-cell neural activity in ocular dominance columns and orientation columns of the cat visual cortex (see the figure). With this arrangement, the investigators were able to simultaneously measure electrophysiological changes and alterations in tissue oxygenation in response to stimuli of different orientations. An optimal orientation stimulus produced a biphasic time course of changes in local tissue oxygenation, which first decreased and then increased before returning to baseline (see the figure). For



**Changes in tissue oxygen content during and after neural activation.** Combined electrodes for measuring neural activity and tissue oxygen content (D) are placed in the orientation columns (C) of the cat visual cortex (B). Different grating patterns are presented to the cat at different orientations (A), and the responses to the different stimuli are measured. When the electrode is positioned in a column optimally sensitive to the orientation of the stimulus grating, the time course of neural activity shows vigorous spiking (E). The corresponding time course of changes in tissue oxygenation (F) shows an initial brief dip followed by a positive overshoot. (G) The initial dip in tissue oxygen content (blue) is due to increased neural activity, whereas the subsequent rise in tissue oxygenation (red) reflects an increase in blood flow. The E and F time courses on the right-hand side depict the response to a grating presented in an orientation orthogonal to the preferred orientation. In this case, there is no neural activity associated with the presentation of the stimulus, and the increase in tissue oxygenation (due to increased blood flow to adjacent columns containing activated neurons) is missing the initial dip.

The author is in the Department of Psychology, University of Sheffield, Sheffield S10 2TP, UK. E-mail: j.e.mayhew@shef.ac.uk

stimuli not at an optimal orientation, the neural response decreased and eventually disappeared completely when the stimulus was in an orientation orthogonal to the preferred orientation. Essentially, Thompson *et al.* reveal that there are two competing processes—the first is a local decrease in tissue oxygenation due to the increased metabolic demand of the activated neurons; the second is a delayed influx of larger amounts of oxygen into tissue comprising both the activated cortical orientation columns and neighboring regions.

The correspondence between increased neural activity and an “early dip” in tissue oxygenation provides strong evidence that activated neurons do indeed, at least in part, satisfy their increased metabolic demand by increased consumption of oxygen. The delayed increase in tissue oxygenation reflects what has been termed “the overwatering of the rose garden” (4)—that is, the area of increased blood flow (hyperemia) is greater than the more localized metabolic effect of neural activity causing it, which results in a “hyperemic overshoot.” In this regard, the Thompson *et al.* work is a pow-

erful and direct confirmation of the interpretation of previous optical imaging spectroscopy and MRI studies (11).

Perhaps it seems that we are ready to close an important chapter on neuronal metabolism research. The Thompson *et al.* work, however, reveals that there are still major gaps in our understanding of neuronal metabolism, with important consequences for interpreting BOLD fMRI signals. There is considerable heterogeneity, for example, in the density of brain capillaries and in the distribution of mitochondria responsible for aerobic metabolism, potentially confounding the interpretation of BOLD fMRI signals and preventing the reliable comparison of signals between different brain regions. We need to elucidate the relationship between changes in the intensity and duration of stimulation, the resultant changes in neural activity, and associated changes in metabolic demand. Next, we need to determine how neural activity and metabolic demand affect the magnitude and timing of the hemodynamic response and of BOLD fMRI measurements.

The Thompson *et al.* work is an important confirmation of a hypothesis about the metabolic activity of activated neurons. Furthermore, their study helps to elucidate the intrinsic signals underlying BOLD fMRI measurements. However, much work remains to be done before we fully understand the relationship between BOLD measurements and the neural interactions underlying them. As a starting point, we could do with an influx of more research funds!

#### References

1. J. K. Thompson, M. R. Peterson, R. D. Freeman, *Science* **299**, 1070 (2003).
2. S. G. Kim, S. Ogawa, *Curr. Opin. Neurobiol.* **12**, 607 (2002).
3. R. D. Frostig, E. E. Lieke, D. Ts'o, A. Grinvald, *Proc. Natl. Acad. Sci. U.S.A.* **87**, 6082 (1990).
4. D. Maloney, A. Grinvald, *Science* **272**, 551 (1996).
5. M. Jones, J. Berwick, D. Johnston, J. Mayhew, *NeuroImage* **13**, 1002 (2001).
6. T. Ernst, J. Hennig, *Magn. Reson. Med.* **32**, 146 (1994).
7. R. S. Menon *et al.*, *Magn. Reson. Med.* **33**, 453 (1995).
8. D. S. Kim, T. Q. Duong, S. G. Kim, *Nature Neurosci.* **3**, 164 (2000).
9. I. Vanzetta, A. Grinvald, *Science* **286**, 1555 (1999).
10. B. M. Ances, D. F. Wilson, J. H. Greenberg, J. A. Detre, *J. Cereb. Blood Flow Metab.* **21**, 511 (2001).
11. R. Buxton, *NeuroImage* **13**, 953 (2001).

#### BIOCHEMISTRY

## How Iron Activates O<sub>2</sub>

Julie A. Kovacs

Several critical processes in biology involve dioxygen (O<sub>2</sub>), and most of these processes are promoted by transition-metal ions. Dioxygen serves, for example, as the electron sink that drives the conversion of electrochemical to chemical energy in our bodies. It is also the oxidant and/or oxygen atom source for the biosynthesis of important biomolecules, including DNA, serotonin, fatty acids, and steroids, and for the breakdown of drugs and other foreign substances in our livers. Reports on pages 1039 and 1037 of this issue (1, 2) shed light on some of the intermediates that may be involved in reactions promoted by nonheme iron enzymes.

Dioxygen oxidations are thermodynamically favored (they release energy), but are slow in the absence of a catalyst. Reduced transition-metal ions are ideally suited as catalysts for O<sub>2</sub> oxidation reactions. They readily react with O<sub>2</sub> to afford potent metal-containing oxidants, such as iron-superoxo (Fe<sup>III</sup>-O<sub>2</sub><sup>-</sup>), iron-peroxo (Fe<sup>III</sup>-O<sub>2</sub><sup>2-</sup>), or iron-oxo (Fe<sup>IV</sup>=O and Fe<sup>V</sup>=O) species. Until now, there was only indirect evidence

for the involvement of any of these intermediate metal-oxygen species in reactions catalyzed by nonheme iron enzymes (3–7). Karlsson *et al.* (1) and Rohde *et al.* (2) now reveal the structures of two possible intermediates that may be involved in catalysis by nonheme iron enzymes.

Mechanistic pathways in metalloenzymes (enzymes that rely on transition metals for their catalytic activity) are determined by the electronic and geometric properties of the metal ion and by the surrounding protein environment. The electronic properties of the metal ion are tuned by the coordinated ligands (atoms or molecules bound to the metal) and are subtly altered by hydrogen-bonding interactions with the protein or interactions with nearby metal ions.

For example, replacing the histidine ligand in hemoglobin with a cysteine and placing the iron ion and its coordinated ligands in a slightly less polar protein environment in cytochrome P450 changes the system from a dioxygen carrier to one that activates O<sub>2</sub> and catalyzes the oxidation of unactivated hydrocarbons. If the porphyrin ligand in cytochrome P450 is replaced with four histidines and the metal ion placed closer to the protein surface in superoxide reductase (8, 9), the enzyme no longer ac-

tivates O<sub>2</sub>; rather, it reduces superoxide (O<sub>2</sub><sup>-</sup>, a dangerous cellular toxin) to H<sub>2</sub>O<sub>2</sub>.

A lot of what we know about the intermediates involved in dioxygen activation comes from studies of heme iron enzymes (those that contain iron in a porphyrin cavity). Examples include horseradish peroxidase and cytochrome P450 (10–12) and their synthetic analogs (13). (Synthetic analogs mimic just the metal ion and its coordination environment, providing greater molecular-level detail because the molecules are smaller.) The conjugated porphyrin ligand governs the pathways by which O<sub>2</sub> is activated. It makes low-spin states—an electronic arrangement in which most or all electrons on the metal ion are paired—accessible and stabilizes highly oxidized iron intermediates.

The ligand environment in mononuclear nonheme iron enzymes, such as isopenicillin N synthase (4) and naphthalene dioxygenase, usually consists of a 2-His-1-carboxylate triad (14). The geometry is more flexible than that of heme iron enzymes, allowing for a more diverse chemistry. Low-spin states are less accessible in nonheme iron enzymes, and the formation of two accessible (labile or vacant) sites adjacent to one another is possible. These structural and electronic differences open up reaction pathways that are unavailable to heme iron (3–7). However, in general, the more reactive an intermediate, the more difficult it is to observe. As a result, very few of the intermediates shown in the fig-

The author is in the Department of Chemistry, University of Washington, Seattle, WA 98195, USA. E-mail: kovacs@chem.washington.edu

philic. Treating *t*-butylthiocyanate with Fp<sup>-</sup> brought about a 20% yield of FpCN (17) [Fig. 4 (reaction 4)]. These chemical models validate the feasibility of the proposed biosynthesis of the CN ligand and its transfer from sulfur to iron (18).

In sum, the cysteine residue of HypE undergoes unprecedented biotransformations in serving as the site for dehydration of a carboxamido moiety to CN, in carrying the CN residue, and in transferring the CN to iron. Previously, thiocyanates were rarely encountered in nature. Thiocyanate synthesis in the marine sponge *Axinyssa n. sp.* has been proposed to involve sulfuration of cyanide to give <sup>-</sup>SCN followed by reaction with a sesquiterpene cation (19), although cyanation of a thiol moiety has also been suggested (20, 21).

References and Notes

1. P. M. Vignais, B. Billoud, J. Meyer, *FEMS Microbiol. Rev.* **25**, 455 (2001).
2. M. Frey, J. C. Fontecilla-Camps, A. Volbeda, in *Handbook of Metalloproteins*, A. Messerschmidt, R. Huber, K. Wieghardt, T. Poulos, Eds. (Wiley, New York, 2001), pp. 880–896.
3. R. P. Hausinger, in *Mechanisms of Metallocenter Assembly*, R. P. Hausinger, G. L. Eichhorn, L. G. Marzilli, Eds. (Wiley-VCH, New York, 1996), pp. 1–18.
4. M. Blokesch et al., *Biochem. Soc. Trans.* **30**, 674 (2002).
5. A. Paschos, A. Bauer, A. Zimmermann, E. Zehelein, A. Böck, *J. Biol. Chem.* **277**, 49945 (2002).
6. A. Paschos, R. S. Glass, A. Böck, *FEBS Lett.* **488**, 9 (2001).
7. Materials and methods are available as supporting material on Science Online.
8. J. C. Rain et al., *Nature* **409**, 211 (2001).
9. C. Li, T. J. Kappock, J. Stubbe, T. M. Weaver, S. E. Ealick, *Structure Fold Des.* **7**, 1155 (1999).
10. A. Paschos, S. Reissmann, A. Böck, unpublished data.
11. E. Hochleitner, S. Reissmann, F. Lottspeich, A. Böck, unpublished observations.
12. G. Burkhardt, M. P. Klein, M. Calvin, *J. Am. Chem. Soc.* **87**, 591 (1965).
13. J. R. Van Wazer, S. Norval, *J. Am. Chem. Soc.* **88**, 4415 (1996).
14. Dehydration of citrullines to cyanamides with *p*-toluenesulfonyl chloride and pyridine, i.e., RNHCONH<sub>2</sub> → RNHCN, was reported in a chemical simulation of arginine biosynthesis and the urea cycle (23).
15. For evidence supporting the relevancy of modeling the active site of [NiFe] hydrogenase with Fp complexes, see (24).
16. A. Jungbauer, H. Behrens, *J. Organomet. Chem.* **186**, 361 (1980).
17. Although this reaction may involve nucleophilic displacement by iron of thiolate at the cyano carbon atom, an electron transfer mechanism is also possible.
18. There are two possibilities for the origin of the CO ligands: hydrolysis of a CN ligand and transfer of a carbamoyl group to iron followed by deamination. Hydrolysis of a CN ligand is analogous to the known hydrolysis of iron isocyanides to iron carbonyl complexes (25). Deamination of carboxamido iron complexes is also known (26).
19. J. S. Simpson, M. J. Garson, *Tetrahedron Lett.* **39**, 5819 (1998).
20. A. T. Pham et al. *Tetrahedron Lett.* **32**, 4843 (1991).
21. C. Jimenez, P. Crews, *Tetrahedron* **47**, 2097 (1991).
22. P. Roespordorf, J. Fohlman, *Biomed. Mass Spectrom.* **11**, 601 (1984).
23. D. Ranganathan, R. Rathi, *J. Org. Chem.* **55**, 2351 (1990).
24. C.-H. Lai et al., *J. Am. Chem. Soc.* **120**, 10103 (1998).
25. V. Riera, J. Ruiz, *J. Organomet. Chem.* **384**, 339 (1990).
26. L. Busetto, R. J. Angelici, *Inorg. Chim. Acta* **2**, 391 (1968).

27. We thank the Deutsche Forschungsgemeinschaft and the Fonds der Chemischen Industrie for supporting the research of A.B. and the donors of the Petroleum Research Fund, administered by American Chemical Society, for support of this research (ACS-PRF 37202-AC3, R.S.G. and H.W.).

Supporting Online Material

www.sciencemag.org/cgi/content/full/299/5609/1067/DC1  
Materials and Methods  
References and Notes

2 December 2002; accepted 15 January 2003

# Single-Neuron Activity and Tissue Oxygenation in the Cerebral Cortex

Jeffrey K. Thompson, Matthew R. Peterson, Ralph D. Freeman\*

Blood oxygen level–dependent functional magnetic resonance imaging uses alterations in brain hemodynamics to infer changes in neural activity. Are these hemodynamic changes regulated at a spatial scale capable of resolving functional columns within the cerebral cortex? To address this question, we made simultaneous measurements of tissue oxygenation and single-cell neural activity within the visual cortex. Results showed that increases in neuronal spike rate were accompanied by immediate decreases in tissue oxygenation. We used this decrease in tissue oxygenation to predict the orientation selectivity and ocular dominance of neighboring neurons. Our results establish a coupling between neural activity and oxidative metabolism and suggest that high-resolution functional magnetic resonance imaging may be used to localize neural activity at a columnar level.

Functional magnetic resonance imaging (fMRI) is a powerful tool used for the non-invasive mapping of neural activity in the brain (1–3). Blood oxygen level–dependent (BOLD) fMRI infers neural activity by measuring small changes in deoxyhemoglobin within the brain’s vasculature. Therefore, the coupling between local cerebral hemodynamics and the underlying neural activity is critically important to the interpretation and design of fMRI studies. Increases in neural activity elicit a delayed decrease in deoxyhemoglobin corresponding to a positive change in the BOLD signal (1–4). Most fMRI investigations use this positive BOLD response to map neural activity. However, because the response is also observed from draining veins that are displaced from the sites of activation, the spatial resolution is limited (5–7). Optical imaging and imaging spectroscopy findings suggest that a fast increase in deoxyhemoglobin, occurring before the delayed decrease, may be a better indicator of neural activity (8, 9). This component of the hemodynamic response is often referred to as the “initial dip.” Recent fMRI studies and direct measurements of oxygen tension within the microcirculation have also identified the initial dip (6, 7, 10–12). In studies of the visual cortex, brain imaging maps that emphasize the initial

dip exhibit sharper patches and stripes [characteristic of orientation and ocular dominance columns (13)] relative to functional maps that are based on other signals (6, 8, 9). It has been proposed that the initial dip reflects an increase in oxygen consumption by active cells and is consequently better localized to the site of neural activity (6, 8, 9).

Despite its potential, the existence and interpretation of the initial dip are controversial because it is not always observed using fMRI (14, 15), and its detection using imaging spectroscopy may be confounded by the difficulty in correcting for the wavelength dependence of light scattering in tissue (16, 17). An alternative hypothesis is that changes in blood volume, rather than oxygen consumption, could account for the initial dip (18). Although simultaneous recordings of fMRI signals and neural activity were recently reported in the monkey’s primary visual cortex (4), the analysis focused on the positive BOLD response and used stimuli that were designed to activate a relatively large uniform area of the cortex. Therefore, the studies did not address neural and hemodynamic coupling at a submillimeter spatial resolution.

In our study, we made simultaneous colocalized measurements of tissue oxygenation and single-cell neural activity in area 17 of the cat’s visual cortex. Tissue oxygenation is linked to deoxyhemoglobin through the local oxygen concentration gradient in tissue and through the oxygen-hemoglobin dissociation curve and is therefore expected to reflect the hemodynamic changes measured with fMRI. A quantitative model of cerebral hemody-

Group in Vision Science, School of Optometry, Helen Willis Neuroscience Institute, University of California, Berkeley, CA 94720–2020, USA.

\*To whom correspondence should be addressed. E-mail: freeman@neurovision.berkeley.edu

namics posits that tissue oxygenation and the BOLD response exhibit similar time courses after brief increases in neural activity (19).

We measured tissue oxygenation with a Clark-style polarographic oxygen microelectrode (20) and measured single-cell neural activity simultaneously with an adjacent platinum microelectrode (Unisense A/S). Both sensors were housed within a double-barrel micropipette (21). The field of sensitivity of the oxygen sensor was a sphere approximately 60  $\mu\text{m}$  in diameter. This is smaller than a typical cortical column (300 to 600  $\mu\text{m}$ ) (13) and of the same order of magnitude as the average intercapillary distance in the cat's brain ( $\sim 30 \mu\text{m}$ ) (22).

We used this combined sensor to identify changes in tissue oxygenation that accompany variations in spike rate during standard measurements of orientation selectivity and ocular dominance (21). These visual parameters have a well-established columnar organization with

in the visual cortex (13). Average time courses of both neural and oxygen responses are presented in Fig. 1, A and C, for a representative neuron. Changes in tissue oxygenation (solid lines with dashed lines representing  $\pm 1$  SE) exhibited clear stimulus-induced changes when averaged over a sufficient number of trials. We measured statistically significant oxygen responses for all 21 cells studied ( $P < 0.0005$ ,  $t$  test). Like hemodynamic responses, the time course of the oxygen response exhibited an initial dip followed by a positive peak (Fig. 1, A and C). The transition from dip to peak was delayed by 1.0 to 2.5 s relative to hemodynamic responses measured with optical imaging and fMRI techniques (6–12). A portion of this delay ( $\sim 0.75$  s) can be attributed to the response time of our sensor (21). The remaining time can be attributed to the high resolution and extravascular nature of our oxygen measurements (23).

Neural and oxygen responses were recorded for six orientation conditions in the

dominant eye. Optimal orientation conditions, which elicited large neural responses, gave rise to the largest initial dips and smallest peaks (Fig. 1A). The same relationship was observed for ocular dominance measurements (Fig. 1C). The ocular dominance was estimated with optimally oriented drifting gratings, which were presented separately to each eye. The example cell in Fig. 1 was left eye dominant and exhibited a larger initial dip in response to left eye stimulation than to right eye stimulation (Fig. 1C). These results suggest two competing mechanisms. First, a dip in the oxygen response begins early, as a result of increased oxygen consumption by activated cells. Second, a peak in the oxygen response begins later, presumably as a result of increased blood flow to the activated area of the cortex. These two mechanisms partially overlap in time, and as a result, each response reduces the size of the other. Furthermore, the two mechanisms operate over

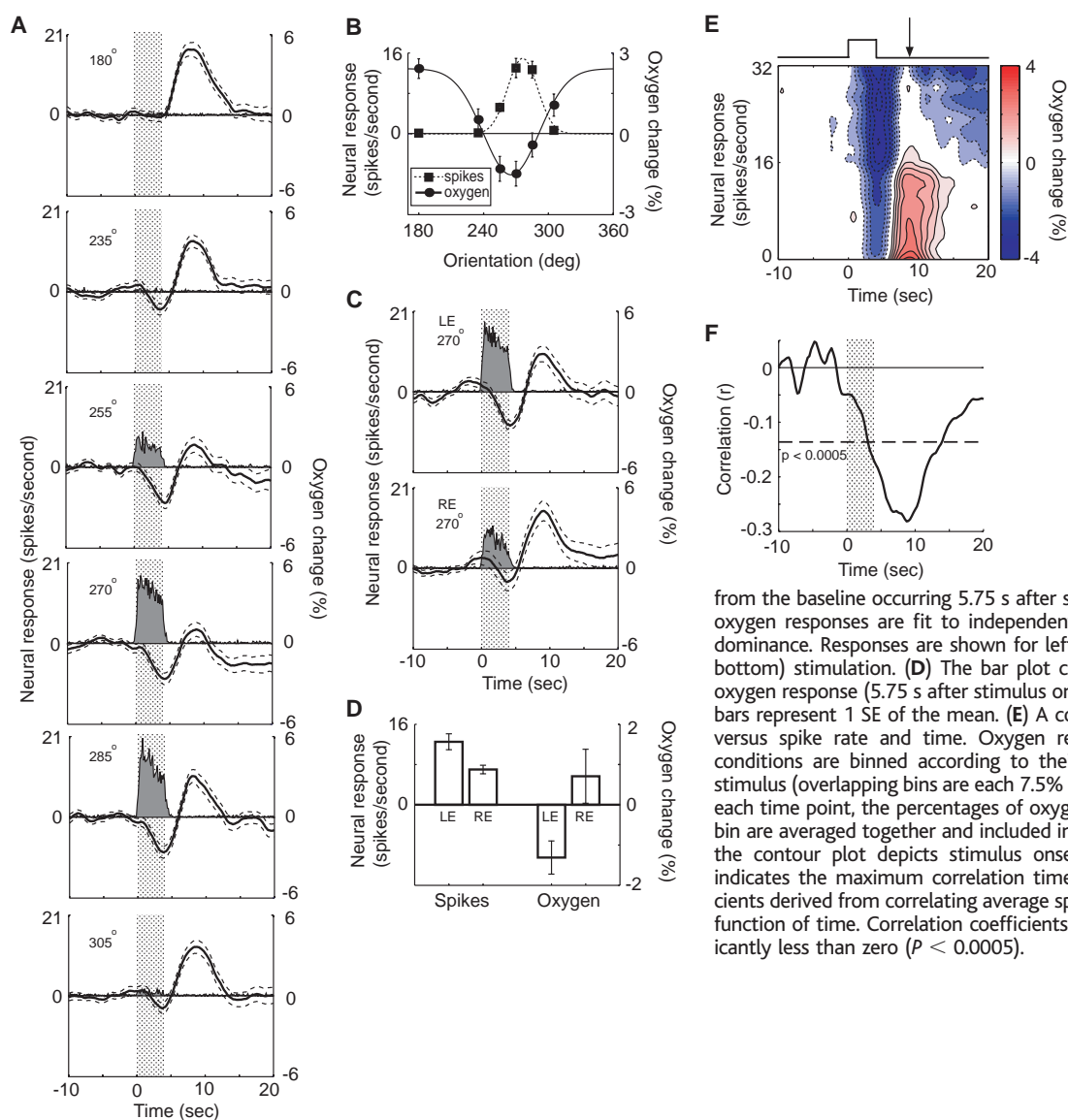


**Fig. 1.** Orientation selectivity, ocular dominance, and correlation analysis for a representative neuron. Spike-time histograms (gray solid area) and oxygen responses (solid lines) in (A) and (C) represent the mean response across 72 trials. All stimuli were drifting sinusoidal gratings presented for 4 s. Gray dotted regions indicate stimulus onset and duration; dashed lines represent 1 SE of the mean. (A) Orientation selectivity. Average responses are shown for six orientation conditions. (B) Comparison between neural and oxygen orientation tuning curves. Spike responses are quantified as the average spike rate during the stimulus, minus the spontaneous rate. Oxygen responses are quantified as the percentage change from the baseline occurring 5.75 s after stimulus onset. Average spike and oxygen responses are fit to independent Gaussian functions. (C) Ocular dominance. Responses are shown for left eye (LE, top) and right eye (RE, bottom) stimulation. (D) The bar plot compares the average neural and oxygen response (5.75 s after stimulus onset) between the two eyes. Error bars represent 1 SE of the mean. (E) A contour plot of tissue oxygenation versus spike rate and time. Oxygen response time courses across all conditions are binned according to their average spike rate during the stimulus (overlapping bins are each 7.5% of the neural response range). For each time point, the percentages of oxygen changes within each response bin are averaged together and included in the contour plot. The line above the contour plot depicts stimulus onset and duration, and the arrow indicates the maximum correlation time (8.75 s). (F) Correlation coefficients derived from correlating average spike rate and oxygen changes as a function of time. Correlation coefficients below the dotted line are significantly less than zero ( $P < 0.0005$ ).

## REPORTS

different spatial scales. We observed the difference in spatial scales in the responses to nonoptimal stimuli, which presumably excited only surrounding columns. The relatively distant activation from neighboring columns elicits a robust peak in the oxygen response without a robust dip. Therefore, the effect of oxygen consumption by active cells was localized within a cortical column, whereas the compensatory inflow of oxygen appears to be spread out over multiple columns.

Orientation tuning curves, derived from neural and oxygen responses in Fig. 1A, gave

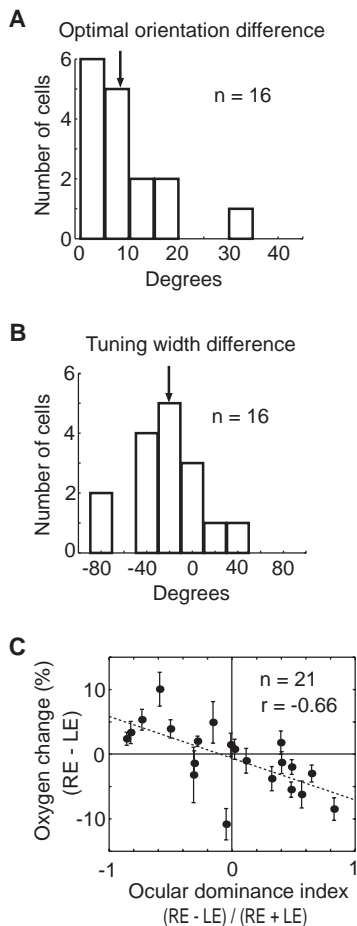


**Fig. 2.** Summary plot of the difference between oxygen and neural measurements of orientation selectivity and ocular dominance. (**A** and **B**) Sixteen of 21 cells had oxygen orientation tuning curves well fit by a Gaussian function ( $r^2 > 0.75$ ). The centers and widths of these 16 fits are compared with the same parameters derived from the neural orientation tuning curves. (**A**) Histogram of the error in predicting optimal orientation selectivity using oxygen responses. The absolute value of each difference is presented. Mean difference (arrow) =  $8.3^\circ$ .  $SD = 8.6^\circ$ . (**B**) Histogram of the error in predicting orientation tuning width from changes in tissue oxygenation. Mean difference (arrow) =  $-20.5^\circ$ .  $SD = 31.2^\circ$ . (**C**) The difference in percent oxygen change between the right and the left eyes is plotted as a function of the ocular dominance index for each neuron.

similar estimates of orientation selectivity (Fig. 1B). The estimates for orientation preference and tuning width differed by  $10.6^\circ$  and  $34.0^\circ$ , respectively. The oxygen tuning curve was inverted because negative changes in the oxygen response corresponded to increases in neural spike rate. Oxygen and neural measurements of ocular dominance, derived from Fig. 1C, exhibited the same relationship (Fig. 1D). Oxygen measurements of orientation tuning and ocular dominance were calculated from the average oxygen change occurring 5.75 s after stimulus onset. This time gave the best correlation between spike rate and tissue oxygenation for the group data (fig. S1). Although the analysis we present here used 5.75 s exclusively, similar results were obtained using times between 4 and 12 s (fig. S2).

A more detailed picture of the predictive relationship between oxygen and neural signals was obtained through correlation analysis (Fig. 1, E and F). The contour plot (Fig. 1E) shows oxygen response time courses as a function of spike rate for the representative neuron. Red and blue shading represent positive and negative changes, respectively, in tissue oxygenation. Trials with high average spike rates have a large dip and a small peak, whereas those with low average spike rates have a small dip and a large peak. Oxygen responses are significantly correlated with spike rate between 3.25 and 14.0 s after stimulus onset (Fig. 1F). During this time period, correlation coefficients are significantly below zero ( $P < 0.0005$ ), indicating an inverse relationship between spike rate and percent of oxygen change.

We studied 21 cells from four cats using the stimulus protocol and analysis methods described above. Tests on 16 of the 21 cells resulted in oxygen orientation tuning curves well fit by a Gaussian function ( $r^2 > 0.75$ ). Of the five cells that did not exhibit orientation tuning in their oxygen responses, three had relatively low neural spike rates. We analyzed these 16 cells further by plotting histograms of the error between neural and oxygen tuning parameters (Fig. 2, A and B). For the majority of cells, the predictions were accurate to within  $15^\circ$  of their optimal orientation (Fig. 2A) and  $40^\circ$  of their tuning width (Fig. 2B). Oxygen orientation tuning curves tended to be wider than neural orientation tuning curves (Fig. 2B). This trend was significant ( $P < 0.05$ ,  $t$  test) and suggests that decreases in tissue oxygenation reflect a population of active cells that have a collective tuning width broader than the tuning width of the individually recorded neuron. The difference between the oxygen responses under right and left eye stimulation showed an inverse relationship when plotted as a function of neural measurements of ocular dominance ( $r = -0.66$ ) (Fig. 2C). This indicates a larger negative percentage of oxygen change in the

stronger eye as compared to the weaker eye.

Previous functional brain imaging studies have proposed that utilization of the initial dip improves the spatial localization of neural activity (6, 8, 9). Our results provide direct evidence for this hypothesis by demonstrating a close relationship between single-unit neural activity and transient decreases in tissue oxygenation. High-resolution fMRI techniques, based on the initial dip, thus have the potential to resolve functional cortical columns that are thought to be fundamental for a wide variety of brain processes.

## References and Notes

1. P. A. Bandettini, E. C. Wong, R. S. Hinks, R. S. Tikofsky, J. S. Hyde, *Magn. Reson. Med.* **25**, 390 (1992).
2. K. K. Kwong *et al.*, *Proc. Natl. Acad. Sci. U.S.A.* **89**, 5675 (1992).
3. S. Ogawa *et al.*, *Proc. Natl. Acad. Sci. U.S.A.* **89**, 5951 (1992).
4. N. K. Logothetis, J. Pauls, M. Augath, T. Trinath, A. Oeltermann, *Nature* **412**, 150 (2001).
5. E. A. Disbrow, D. A. Slutsky, T. P. Roberts, L. A. Krubitzer, *Proc. Natl. Acad. Sci. U.S.A.* **97**, 9718 (2000).
6. D. S. Kim, T. Q. Duong, S. G. Kim, *Nature Neurosci.* **3**, 164 (2000).
7. A. F. Canestra *et al.*, *Cereb. Cortex* **11**, 773 (2001).
8. D. Malonek, A. Grinvald, *Science* **272**, 551 (1996).
9. A. Grinvald, H. Slovov, I. Vanzetta, *Nature Neurosci.* **3**, 105 (2000).
10. N. K. Logothetis, H. Guggenberger, S. Peled, J. Pauls, *Nature Neurosci.* **2**, 555 (1999).
11. E. Yacoub *et al.*, *NMR Biomed.* **14**, 408 (2001).
12. I. Vanzetta, A. Grinvald, *Science* **286**, 1555 (1999).
13. V. B. Mountcastle, *Brain* **120**, 701 (1997).
14. J. J. Marota *et al.*, *Magn. Reson. Med.* **41**, 247 (1999).
15. A. C. Silva, S. P. Lee, C. Iadecola, S. G. Kim, *J. Cereb. Blood Flow. Metab.* **20**, 201 (2000).
16. J. Mayhew *et al.*, *Neuroimage* **10**, 304 (1999).
17. U. Lindauer *et al.*, *Neuroimage* **13**, 988 (2001).
18. R. B. Buxton, E. C. Wong, L. R. Frank, *Magn. Reson. Med.* **39**, 855 (1998).
19. Y. Zheng *et al.*, *Neuroimage* **16**, 617 (2002).
20. I. Fatt, *Polarographic Oxygen Sensors* (CRC, Cleveland, OH, 1976), pp. 197–218.
21. Materials and methods are available as supporting material on Science Online.
22. H. Kanaïwa, H. Kuchiwaki, S. Inao, K. Sugita, *Surg. Neurol.* **44**, 172 (1995).
23. The high-resolution measurements from our combined sensor were localized within the activated areas of the cortex with minimal overlap into nonactivated areas. As a result, we observed a stronger initial dip with an expanded time course. A similar effect is observed in high-resolution BOLD fMRI measurements (6). The time required for oxygen in the vasculature to diffuse into tissue may also contribute to the longer initial dip.
24. Supported by research and CORE grants from the National Eye Institute (EY01175 and EY03176, respectively) as well as an NIH training grant (T32 EY 07043-24). We thank Unisense A/S for cooperation in development of the combined sensor, M. D'Esposito for helpful comments during preparation of the manuscript, S. Bierer and B. Li for helpful discussions and data collection, and L. Altamirano for help with sensor calibration.

## Supporting Online Material

www.sciencemag.org/cgi/content/full/299/5609/1070/DC1  
Materials and Methods  
SOM Text  
Figs. S1 and S2  
References and Notes

8 October 2002; accepted 20 December 2002